Solution Equilibria of Anticancer Ruthenium(II)-(η^6-*p*-Cymene)-Hydroxy(thio)pyr(id)one Complexes: Impact of Sulfur *vs.* Oxygen Donor Systems on the Speciation and Bioactivity

Éva A. Enyedy[a], Éva Sija[a,b], Tamás Jakusch[a*], Christian G. Hartinger[c,d,e], Wolfgang Kandioller[c,e], Bernhard K. Keppler[c,e], Tamás Kiss[a,b*]

[a] Department of Inorganic and Analytical Chemistry, University of Szeged, Dóm tér 7, H-6720 Szeged, Hungary

[b] Bioinorganic Chemistry Research Group of the Hungarian Academy of Sciences, University of Szeged, Dóm tér 7, H-6720 Szeged, Hungary

[c] Institute of Inorganic Chemistry, University of Vienna, Waehringer Str. 42, A-1090 Vienna, Austria

[d] School of Chemical Sciences, The University of Auckland, PB: 92019, 1142 Auckland, New Zealand

[e] University of Vienna, Research Platform Translational Cancer Therapy Research, Waehringer Str. 42, A-1090 Vienna, Austria

Keywords: Stability Constants, Ruthenium Antitumor Complexes, Thiomaltol, Allomaltol, Speciation

* Corresponding authors: Fax: +36 62 420505

E-mail addresses: jakusch@chem.u-szeged.hu (T. Jakusch), tkiss@chem.u-szeged.hu (T. Kiss)

ABSTRACT

Stoichiometry and stability of antitumor ruthenium(II)−η^6-*p*-cymene complexes of bidentate (O,O) hydroxypyrone and (O,S) hydroxythiopyr(id)one type ligands were determined by pH-potentiometry, ^{1}H NMR spectroscopy and UV−Vis spectrophotometry in aqueous solution and in dependence of chloride ion concentration. Formation of mono-ligand complexes with moderate stability was found in the case of the hydroxypyrone ligands (ethyl maltol and allomaltol) predominating at the physiological pH range. These complexes decompose to the dinuclear tri-hydroxido bridged species [{$Ru^{II}(\eta^6$-*p*-cymene}$_2(OH)_3$] and to the metal-free ligand at basic pH values. In addition, formation of a hydroxido [$Ru^{II}(\eta^6$-*p*-cymene)(L)(OH)] species was found. The hydroxythiopyr(id)one ligands (thiomaltol, thioallomaltol, 3-hydroxy-1,2-dimethyl-thiopyridone) form complexes of significantly higher stability compared with the hydroxypyrones; their complexes are biologically more active, the simultaneous bi- and monodentate coordination of the ligands in the bis complexes (ML_2 and ML_2H) was also demonstrated. In the case of thiomaltol, formation of tris complexes is also likely at high pH. The replacement of the chlorido by the aqua ligand in the [$Ru^{II}(\eta^6$-*p*-cymene)(L)(Cl)] species was monitored, which is an important activation step in the course of the mode of action of the complexes, facilitating binding to biological targets.

1. Introduction

Anticancer metallodrug research has been initiated by the discovery and clinical success of cis-diamminedichloridoplatinum(II), cisplatin. However, the limited activity, adverse effects and resistance phenomena of the Pt-based drugs in the clinics are well known, which justifies the development and evaluation of other types of metal complexes with anticancer activity. The two Ru(III) complexes imidazolium trans-[tetrachlorido(dimethylsulfoxide)(1*H*-imidazole)ruthenate(III)] (NAMI-A) and sodium trans-[tetrachloridobis(1*H*-indazole)ruthenate(III)] (KP1339) are currently undergoing clinical trials with promising results [1-3]; however, antitumor properties of Ru complexes were already reported in the 1950s [4]. In the last decade, numerous organometallic ruthenium(II)-η^6-arene complexes mainly with piano-stool structure were synthesized and tested in *in vitro* assays regarding their bioactivity. In these Ru^{II} complexes the facial arene moiety results protects the metal center against oxidation. A large number of [Ru^{II}(η^6-*p*-cymene)(XY)Cl]-type compounds was prepared, where XY is an (*O*,*O*), (*O*,*S*), (*O*,*N*), (*N*,*N*) or (*N*,*S*) bidentate ligand [5-12]. The chloride ligand acts a leaving group and its replacement by a water molecule facilitates the reaction with biological targets. Although, the ultimate biotarget of these [Ru^{II}(η^6-*p*-cymene)(XY)Cl] complexes is still unclear [13,14], DNA is considered to be a potential intracellular target [9,15].

Ru^{II}(arene)Cl complexes can be regarded as prodrugs and it is a prerequisite to follow their speciation in biological fluids for a better understanding of the pharmacokinetic properties and the mechanism of action. Equilibrium studies are a first approach to characterize their properties in aqueous solution. The substitution of original chelating ligands by endogenous biomolecules has a major impact on the integrity of the complexes and their presence in the biologically active form fundamentally depends on the thermodynamic stability and kinetic inertness/lability. Only little information is available in the literature about the solution speciation of ruthenium(II)-η^6-arene complexes: on the formation of complexes with bidentate (O,O) ligands was studied [16] and pK_a values of the coordinated water molecule in [Ru^{II}(η^6-*p*-cymene)(XY)(H_2O)] species were determined for several XY bidentate ligands [5,17-19]. Complexes of hydroxypyrones (such as the well-known 3-hydroxy-2-methyl-4H-pyran-4-one (maltol)) show only moderate cytotoxicity on various cancer cell lines as compared with the more active (O,S) type complexes of hydroxythiopyrones [5]. In order to establish structure-*stability*-activity relationships the characterization of the stability of these complexes, the knowledge of the speciation and the

most plausible chemical forms in aqueous solution is mandatory. Therefore, we performed detailed pH-potentiometric, UV-Vis spectrophotometric and ^{1}H NMR spectroscopic measurements to investigate the stoichiometry and stability of the [Ru^{II}(η^6-*p*-cymene)] complexes of hydroxypyrone (2-ethyl-3-hydroxy-4-pyranone (ethyl maltol), 5-hydroxy-2-methyl-4H-pyran-4-one (allomaltol)) and hydroxythiopyr(id)one (3-hydroxy-2-methyl-4-thiopyrone (thiomaltol), 5-hydroxy-2-methyl-4-thiopyrone (thioallomaltol), 3-hydroxy-1,2-dimethyl-thiopyridone (thiodhp) ligands (Chart 1). The chlorido/aqua co-ligand exchange reaction in the [Ru^{II}(η^6-*p*-cymene)(L)(Cl)] species was also monitored. Stability constants of the complexes were determined in the presence and in the absence of chloride ions.

Chart 1

2. Experimental

2.1. Chemicals

Ethyl maltol, KCl, KNO_3, $AgNO_3$, HCl, HNO_3 and KOH were purchased from Sigma-Aldrich and used without further purification. Allomaltol [20], thiomaltol [21], thioallomaltol [22] and thiodhp [21] were prepared according to literature procedures. The purity of the ligands was checked and the exact concentration of the ligand stock solutions was determined by pH-potentiometric titrations with the help of the computer program HYPERQUAD [23]. [Ru^{II}(η^6-*p*-cymene)Cl_2]$_2$ was synthesized and purified according to a literature procedure [24]. A stock solution of [Ru^{II}(η^6-*p*-cymene)Z_3] (where Z = H_2O and/or Cl^-; charges are omitted for simplicity) was obtained by dissolving a known amount of [Ru^{II}(η^6-*p*-cymene)Cl_2]$_2$ in water, while the stock solution of [Ru^{II}(η^6-*p*-cymene)$(H_2O)_3$]$(NO_3)_2$ was obtained from a solution of [Ru^{II}(η^6-*p*-cymene)Cl_2]$_2$ in water after removal of chloride ions using equivalent amounts of $AgNO_3$. The exact concentration of the [Ru^{II}(η^6-*p*-cymene)Z_3] stock solutions (with or without chloride) was determined by pH-potentiometric titrations employing literature data for [Ru_2(η^6-*p*-cymene)$_2$(hydroxido)$_i$] (i = 2 or 3) complexes [16,25].

2.2. pH-potentiometric measurements

The pH-potentiometric measurements for determination of the protonation constants of the ligands and the overall stability constants of the metal complexes were carried out at 25.0 ± 0.1 °C in water and at an ionic strength of 0.20 M KCl (for all the systems studied) or KNO_3 (in the case of ethyl maltol) in order to keep the activity coefficients constant. The titrations were performed with carbonate-free KOH solution (0.20 M). The exact concentrations of HCl, HNO_3 and KOH solutions were determined by pH-potentiometric titrations. An Orion 710A pH-meter equipped with a Metrohm combined electrode (type 6.0234.100) and a Metrohm 665 Dosimat burette were used for the pH-potentiometric measurements. The electrode system was calibrated to the pH = $-\log[H^+]$ scale by means of blank titrations (strong acid *vs.* strong base: HCl/HNO_3 *vs.* KOH), as suggested by Irving *et al.* [26]. The average water ionization constant, pK_w, was determined as 13.76 ± 0.01 at 25.0 °C, I = 0.20 M (KCl, KNO_3), which corresponds well to the literature [27]. The reproducibility of the titration points included in the calculations was within 0.005 pH. The pH-potentiometric titrations were performed in the pH range 2.0−11.5. The initial volume of the samples was 10.0 mL. The ligand concentration was 2.0 mM and metal ion-to-ligand ratios of 1:1 to 1:3 were used. The accepted fitting of the titration curves was always less than 10 μL. Samples were degassed by bubbling purified argon through them for *ca.* 10 min prior to the measurements and it was also passed over the solutions during the titrations.

The computer program PSEQUAD [28] was utilized to establish the stoichiometry of the complexes and to calculate the overall stability constants. $\beta(M_pL_qH_r)$ is defined for the general equilibrium $pM + qL + rH \rightleftharpoons M_pL_qH_r$ as $\beta(M_pL_qH_r) = [M_pL_qH_r]/[M]^p[L]^q[H]^r$ where M denotes the metal moiety $[Ru^{II}(\eta^6\text{-}p\text{-cymene})Z_3]$ and L the completely deprotonated ligand. Literature $\log\beta$ values of the various $[Ru^{II}(\eta^6\text{-}p\text{-cymene})(\text{hydroxido})]$ complexes were used in the absence and presence of chloride ions [16,25] and compared to data collected in the course of the experiments described herein. In all calculations exclusively titration data were used from experiments in which no precipitate was visible in the reaction mixture.

2.3. UV–Vis spectrophotometric and ^{1}H NMR measurements

A Hewlett Packard 8452A diode array spectrophotometer was used to record the UV-Vis spectra in the interval 200–800 nm. The path length was 1 cm. Protonation and stability constants and the individual spectra of the species were calculated with the computer program PSEQUAD [28]. The spectrophotometric titrations were performed on samples of the ligands

alone or with [$Ru^{II}(\eta^6$-*p*-cymene)Z_3] over the pH range 2.0–11.5 at an ionic strength of 0.20 M (KCl or KNO_3) and at 25.0 ± 0.2 °C. The concentration of ligands was set constant at 0.12 mM and the metal-to-ligand ratios were 1:1, 1:2 and 1:3. UV-Vis spectra of samples containing the [$Ru^{II}(\eta^6$-*p*-cymene)Z_3] and the thioallomaltol were also recorded at various ratios (1:1.5−1:3) at constant concentration of the metal ion (0.04 mM) at pH 9.0 at an ionic strength of 0.20 M KCl under anaerobic conditions.

UV-Vis measurements for [$Ru^{II}(\eta^6$-*p*-cymene)Z_3]−hydroxythiopyr(id)one systems were carried out at 1:1 metal-to-ligand ratio by preparing individual samples in which KCl was partially or completely replaced by HCl and pH values varying in the range ca. 0.9–2.0 were calculated from the HCl content.

^{1}H NMR studies were carried out on a Bruker Ultrashield 500 Plus instrument. 4,4-Dimethyl-4-silapentane-1-sulfonic acid was used as an internal NMR standard. The ligands were dissolved in a 10% (v/v) D_2O/H_2O mixture to yield a concentration of 2 mM and were titrated at 25 °C, at I = 0.20 M (KCl, KNO_3) in absence or presence of [$Ru^{II}(\eta^6$-*p*-cymene)Z_3] at 1:1, 1:2 and 1:3 metal-to-ligand ratios. Samples containing [$Ru^{II}(\eta^6$-*p*-cymene)Z_3] and hydroxythiopyr(id)one ligands at various ratios (1:1−1:5) at constant concentration of the ligand (2 or 3 mM) at pH 3.0 and 9.0 were also measured. The ^{1}H NMR spectra were recorded to study the H_2O/Cl^- exchange processes in the [$Ru^{II}(\eta^6$-*p*-cymene)(L)Z] complexes for ethyl maltol at pH 3.0, for allomaltol at pH 5.5, and for the thioallomaltol at pH 2.1, 6.0 and 9.0 in dependence of the Cl^- concentration (4−500 mM). Protonation and stability constants were calculated with the computer program PSEQUAD [28].

2.4. DFT calculations

The structure of complex [ML_2] of thiomaltol was geometry-optimized to energy minimum convergence with Gaussian 09 [29], using restricted DFT. The non-local Becke three-parameter hybrid functional (rB3LYP) method was applied [30-32] and a 6-31+G(d,p) basis set was employed for the geometry optimization and frequency analysis of non-metal atoms [33] and the quasi-relativistic Stuttgart/Dresden energy-consistent pseudo-potentials basis set (SDD-ECP) for the Ru center [34]. All models represent an energy minimum on the potential energy surface as confirmed by absence of imagery (negative) frequencies. The graphical representation was prepared with GaussView 5.0.8 [35].

3. Results and discussion

3.1. Proton dissociation processes of the ligands

Recently, we reported the pK_a values of allomaltol, thiomaltol and thioallomaltol (Chart 1, Tables 1,2) obtained under identical conditions (at 25 °C, I = 0.20 M (KCl)) as used in this study [36] with the exception of ethyl maltol and thiodhp, and the values determined in the course of the current experiments are in good agreement to them. The proton dissociation constants of hydroxy(thio)pyr(id)ones can be attributed to the deprotonation of the hydroxyl functional group, whereas, in contrast to dhp, thiodhp (pK_a = 9.46 at I = 0.2 M KCl, pK_a = 9.47 at I = 0.1 M KCl [37]) is not protonated in the pH range 2–11.5. This is most probably attributable to the unfavorable catechol-type tautomeric form [38] in the case of thiodhp [39]. The pK_a of ethyl maltol determined by pH-potentiometric, UV-Vis spectrophotometric and ^{1}H NMR titrations (pK_a = 8.54; Tables 1 and S1) was found to be slightly higher compared with maltol (pK_a = 8.45) [16,36]. Similar to maltol, the deprotonation of ethyl maltol is accompanied by a characteristic shift of the λ_{max} value from 276 nm (ε_{276} = 7260 $M^{-1}cm^{-1}$) to 320 nm (ε_{320} = 6850 $M^{-1}cm^{-1}$). It is noteworthy that the sulfur-containing derivatives possess 0.3-0.5 log units lower pK_a values as compared with the corresponding reference compounds, while the deprotonation of the allo derivatives always takes place at a considerably lower pH range. Additionally, the thio ligands are significantly more lipophilic than the hydroxypyrone analogues [36].

Table 1

Table 2

3.2. Solution equilibria of [$Ru^{II}(\eta^6$-p-cymene)Z_3] complexes of hydroxypyrones

The complex formation processes of ethyl maltol with $[Ru^{II}(\eta^6\text{-}p\text{-cymene})(H_2O)_3]^{2+}$ were studied by pH-potentiometry, UV-Vis spectrophotometry and ^{1}H NMR spectroscopy in the presence of 0.2 M KNO_3. The hydrolytic equilibrium of the organometallic moiety was found to be fast and simple in the absence of chloride. The stability constant of the dinuclear hydrolysis product $[Ru_2(\eta^6\text{-}p\text{-cymene})_2(OH)_3]^+$ was determined by pH-potentiometric and UV-Vis spectrophotometric titrations of $[Ru^{II}(\eta^6\text{-}p\text{-cymene})(H_2O)_3]^{2+}$ (Table 1) as logβ (M_2H_{-3}

$_3$) = -9.36(2) and -9.33(2), respectively, which are also in good agreement with data obtained by Buglyó *et al.* [25].

The complex formation with ethyl maltol starts already in the acidic pH range and the stability constant of the complex $[Ru^{II}(\eta^6\text{-}p\text{-cymene})(L)(H_2O)]^+$ (denoted $[ML]^+$) was determined by pH-potentiometry and by UV-Vis spectrometry following the changes of the charge transfer (CT) bands, and the data are in good agreement with each other (Table 1). In this mono-ligand complex the bidentate (*O*,*O*) coordination mode of the ligand is the most feasible in solution, similarly to other hydroxypyrone compounds [6], as demonstrated also by single-crystal X-ray diffraction studies [40]. The chemical shifts of the protons of the ligand and the $[Ru^{II}(\eta^6\text{-}p\text{-cymene})]$ moiety being bound or free are clearly distinguishable in the ^{1}H NMR spectra due to the slow exchange processes ($t_{1/2}$(obs) > ~1 ms) with respect to the NMR time scale (Fig. 1).

Fig. 1

The spectral changes clearly show that two overlapping processes take place at pH > ~8.8, namely i) the formation of a mixed hydroxido species $[Ru^{II}(\eta^6\text{-}p\text{-cymene})(L)(OH)]$ resulting in a significant upfield shift of the peaks and ii) the dissociation of the complex $[ML]^+$ according to equation (1).

$$2\ [Ru(\eta^6\text{-}p\text{-cymene})(L)(H_2O)]^+ + H_2O \rightleftharpoons [Ru_2(\eta^6\text{-}p\text{-cymene})_2(OH)_3]^+ + 2\ L^- + 3\ H^+ \quad (1)$$

The latter process was found to be relatively slow and could not accurately be followed by pH-potentiometry as the real equilibrium could not be reached during the time-scale of this method. The pK_a value for the deprotonation of the species $[ML]^+$ was estimated on the basis of the pH-dependence of the signals of the C*H*(Ar) cymene protons in the ^{1}H NMR spectra (Table 1; Fig. 1), which is similar to the value published previously [5].

Chloride ions are coordinative ligands for ruthenium(II) in aqueous solution, and therefore hydrolysis and complex formation of $[Ru^{II}(\eta^6\text{-}p\text{-cymene})(H_2O)_3]^{2+}$ become more complicated in the presence of chloride ions. Various aqua, chlorido, hydroxido and mixed chlorido-hydroxido/aqua complexes are present at acidic pH ($[Ru(\eta^6\text{-}p\text{-cymene})(H_2O)_3]^{2+}$, $[Ru(\eta^6\text{-}p\text{-cymene})(H_2O)(Cl)]^+$, $[Ru_2(\eta^6\text{-}p\text{-cymene})_2(OH)_nCl_{3-n}]^+$ where n = 0–3), whereas above pH ~6.5 the dinuclear complex $[Ru_2(\eta^6\text{-}p\text{-cymene})_2(OH)_3]^+$ predominates [17]. It should be noted that chloride suppresses the hydrolysis and shifts it to the higher pH range.

The hydrolysis at 0.2 M KCl ionic strength can be described reasonably well with the formation of the dimeric species $[Ru_2(\eta^6\text{-}p\text{-cymene})_2(OH)_2Z_2]^{2+}$ and $[Ru_2(\eta^6\text{-}p\text{-cymene})_2(OH)_3]^{+}$ and their stability constants determined in this work by pH-potentiometry and UV-Vis spectrometry (Table 1) are in a good agreement with literature data [16,17].

The complexation of ethyl maltol and allomaltol with $[Ru^{II}(\eta^6\text{-}p\text{-cymene})Z_3]$ in the presence of chloride exhibits similarities as in the absence of chloride (vide supra), namely formation of [ML] and $[MLH_{-1}]$ was found; however some discrepancies were undoubtedly observed. First of all, the possible substitution of the aqua ligand by chlorido in the $[Ru^{II}(\eta^6\text{-}p\text{-cymene})Z_3]$ and $[Ru^{II}(\eta^6\text{-}p\text{-cymene})(L)Z]$ (= [ML]) species needs to be taken into consideration. Therefore, all the stability data determined in the presence of chloride are regarded as conditional stability constants and are valid only under the given conditions (0.2 M KCl, T = 25 °C). On the other hand, chloride as a competitive ligand has effect on the stabilities as well. The overall stability constants of the species [ML] formed with ethyl maltol and allomaltol were determined by pH-potentiometry and by UV-Vis spectrophotometry based on the spectral changes (Table 1, Fig. 2).

Fig. 2

The pH-dependence of the ^{1}H NMR spectra of the $[Ru^{II}(\eta^6\text{-}p\text{-cymene})Z_3]$–ethyl maltol and –allomaltol systems was studied over a wide pH range and representative spectra are shown in Fig. 3. The formation of a complex [ML] can be recognized already at pH ~2, however its molar fraction is significantly lower in the presence of chloride than in its absence (c.f. Fig. 1), indicating somewhat lower stabilities in this milieu.

Fig. 3

Due to the well-separated ^{1}H NMR signals of the protons belonging to the bound and non-bound ligand and *p*-cymene, the integrated areas of the corresponding peaks can be calculated and converted to molar fractions. Molar fractions were also calculated under the same conditions based on the stability constants obtained by pH-potentiometry (see Fig. 4 for allomaltol). A good correlation between the data of the two methods was observed when collected at pH < 8, whereas under more basic conditions deviations were observed. Most probably the system was not in an equilibrium state during the pH-potentiometric titrations in the basic pH range due to the slow dissociation of the complex [ML]. However, it was found that the hydrolysis of the species [ML] starts at somewhat lower pH than the complex dissociation in the case of ethyl maltol, which allowed the calculation of the stability constant of $[MLH_{-1}]$ based on pH-potentiometry data. Furthermore, pK_a values for the species [ML] of

allomaltol and ethyl maltol were also estimated based on the shift of the C*H*(Ar) *p*-cymene proton signals in ^{1}H NMR spectra (Table 1).

Fig. 4

Formation of bis-ligand complexes could be undoubtedly excluded via recording the pH-dependence of the ^{1}H NMR spectra at ligand excess (at M:L = 1:2). These spectra (not shown) consist of peaks, which could be assigned persuasively to the species which are present at the titrations of samples with 1:1 metal-to-ligand ratio.

Direct comparison of the cumulative stability constants of the complexes [ML] of ethyl maltol and allomaltol (Table 1) with that of maltol [17] reveals the following order: allomaltol < ethyl maltol < maltol. In order to take into consideration the different basicities of the ligands the logβ values were corrected according to the competition reaction equations (2; Z = H_2O or Cl^-) and (3).

$$[Ru^{II}(\eta^6\text{-}p\text{-cymene})Z_3] + HL \rightleftharpoons [Ru^{II}(\eta^6\text{-}p\text{-cymene})(L)Z] + H^+ + 2\,Z \qquad (2)$$

$$\log K^* = \log\beta\,[Ru^{II}(\eta^6\text{-}p\text{-cymene})(L)Z] - pK_a(HL) \qquad (3)$$

Log*K** values of 0.60, 0.45 and 0.38 were obtained for maltol, ethyl maltol and allomaltol, respectively, demonstrating that the position of the ring methyl group has a distinct influence on the speciation. However, the complex of the allomaltol derivative is somewhat less stable than its Ga^{III} complexes [36]. On the other hand, the exchange of the methyl group of maltol to ethyl also results in a small decrease in stability, although these differences are minor. It should also be noted that the stability of complexes formed with 3,4-hydroxypyridones (such as 3-hydroxy-1,2-dimethyl-pyridone (deferiprone) is higher than with these hydroxypyrones [17], which in turn are more stable than with 3-hydroxy-2-pyridone ligands [41] compared. The increased stability of deferiprone complexes is related to its coordination in the chatecolate-type tautomeric form, where the ring is aromatic and the nitrogen is (at least partly) positively charged.

In $[Ru^{II}(\eta^6\text{-}p\text{-cymene})(L)(H_2O)]^+$ the third coordination site is most probably occupied by a water molecule in the absence of chloride, although it can be partially (or completely) displaced by a chlorido ligand in KCl-containing milieu or *vice versa* the chlorido complex may undergo aquation after dissolution. As a fast equilibrium occurs between the complex with chlorido or aqua ligands (no separated signals in ^{1}H NMR spectra), the extent of Cl^-/H_2O exchange cannot be judged from NMR spectra recorded at a particular chloride concentration.

Therefore, spectral changes of the $[Ru^{II}(\eta^6\text{-}p\text{-cymene})(L)(H_2O)]^+$ were followed by ^1H NMR spectroscopy at various chloride concentrations at pH 3.5 and 5.5, at which the species [ML] predominate in case of ethyl maltol and allomaltol, respectively. A small, but well-defined shift of the NMR signals was observed related to the coordination of Cl^- to the Ru center. Based on the changes of chemical shifts, the stepwise stability constants could be estimated for the H_2O/Cl^- co-ligand exchange equilibria (Fig. S1, Table 1). According to these data about 36% and 52% of the ethylmaltol complex [ML] are chlorinated at 0.1 and 0.2 M chloride concentrations, respectively, while for allomaltol approximately 44% and 61% of the chlorido species were found at the pH values studied.

3.3. Solution equilibria of $[Ru^{II}(\eta^6\text{-p-cymene})Z_3]$ complexes of hydroxythiopyr(id)ones

The complex formation processes of thiomaltol, thioallomaltol and thiodhp (Chart 1) with $[Ru^{II}(\eta^6\text{-}p\text{-cymene})Z_3]$ were studied by a combined approach of pH-potentiometry, ^1H NMR and UV-Vis spectrophotometry in aqueous solution in the presence of 0.2 M chloride. Since hydroxythiopyr(id)ones can undergo oxidation, anaerobic conditions were used for the measurements.

The pH-potentiometric titration curves recorded at 1:1 metal-to-ligand ratio show the complete proton displacement by the metal ion already at the starting pH value (i.e. pH 2), which hampers the determination of the stability constant of the mono-ligand complex formed under these conditions (see Chart 2). It was also observed that a slow process starts resulting in proton liberation at pH > ~6 (with the exception of the thiodhp system), which finally leads to the appearance of precipitate. In addition, UV-Vis spectra of the $[Ru^{II}(\eta^6\text{-}p\text{-cymene})Z_3]$–hydroxythiopyr(id)one systems at 1:1 metal-to-ligand ratio were recorded in the pH range 2.0-11.5, and complemented by studies with samples, in which the KCl was partially or completely replaced by HCl to maintain the ionic strength constant in the pH range 0.9–2.0 (Fig. 5).

Fig. 5

The spectra recorded in the pH 0.9-6.0 range were found to be identical, but are unambiguously different to the spectra of the metal-free ligand or the non-bound $Ru^{II}(\eta^6\text{-}p\text{-}$cymene) moiety. This finding strongly suggests the formation of one kind of species, most probably complex [ML]; however its stability constant cannot be calculated, since it predominates at pH 0.9-6.0 and no complex dissociation seems to take place by decreasing

the pH. Therefore, only a threshold limit could be estimated for the logβ of complex [ML] (Table 2). At the same time, the character of the UV-Vis spectra changes at pH > 6 and a significant decrease of the absorbance is observed in the 230-530 nm wavelength range. The ^{1}H NMR spectra measured at 1:1 metal-to-ligand ratio at various pH values show the same picture about the speciation, namely only one kind of complex predominates in the acidic pH range (Fig. S2); though the intensity of the signal is strongly diminished at pH > ~5.5. Most probably the species [ML, L = thiomaltol or allothiomaltol] starts to hydrolyze via the formation of poorly water-soluble ternary hydroxido oligomers or polymers, unlike in the case of the ligands with (O,O) donor atoms (vide supra). In contrast, no hydrolysis or precipitation processes were observed with thiodhp. Its complex [ML] predominates practically in the whole pH range as the ^{1}H-NMR spectra are identical at pH 2.0 and pH 10.5.

The speciation in the [Ru^{II}(η^6-p-cymene)Z_3]–hydroxythiopyr(id)one systems was found to be different and more complicated at ligand excess. The pH-potentiometric titrations clearly showed that an excess of ligand is able to protect the metal ion against the hydrolysis up to pH 10. Careful analysis of the ^{1}H NMR spectra recorded at various metal-to-ligand ratios reveals in all cases formation of bis-ligand complexes besides the respective species [ML]. Representative spectra are shown for the [Ru^{II}(η^6-*p*-cymene)Z_3]–thioallomaltol system at pH 3.0 in Figure 6 (Fig. S3 for thiomaltol).

Fig. 6

The exclusive formation of [ML] is seen at 1:1 ratio (c.f. Fig. S2). A new set of peaks was detected at higher ppm values compared with those of species [ML] when the ligand excess is increased and their position is unchanged up to ca. 1:2 metal-to-ligand ratio. Then they start to broaden and shift to the direction of the peaks of the metal-free ligand. On the other hand, the peaks belonging originally to [ML] become broader and are upfield shifted, and their positions remain constant at higher than M: L = 1:2 ratio ligand excess. These observations can be explained by the possible formation of a bis-ligand complex, in which one of the ligands is coordinated through the (O,S) donor set, but the other one binds in a monodentate manner via the thione-sulfur to the third available coordination site (3 coordination sites in pseudo octahedral piano-stool compounds are occupied by π-bonded *p*-cymene; Chart 2). Bis-ligand complex of 2-pyridinethiol formed with [Ru^{II}(η^6-C_6Me_6)] at ligand excess also represents the bidentate (N_{pyr},thiol-S) and monodenate (thiol-S) coordination of the ligands [42].

Chart 2

The most probable composition of this complex is $[ML_2H]$ at pH 3.0. The ligands coordinating in a bidentate mode in the species [ML] and $[ML_2H]$ are in a fast exchange with respect to the NMR time scale resulting in signal broadening. However, the peaks become sharp at ligand excess (metal : ligand > 1:2) leading to the formation of $[ML_2H]$ over [ML]. The protonated ligands coordinating monodentately in $[ML_2H]$ and the metal-free ligand (HL) are also in a fast exchange at a ratio higher than ~1:2, when the non-bound HL becomes detectable. The same behavior was observed for thiomaltol (Fig. S3). The speciation model is the same as for thiodhp, although the ligand exchange rates are slower. The peaks for the chelating ligand in the species [ML] and $[ML_2H]$ are distinct and sharp. However, a broad signal set represents that the free ligand and the ligand in $[ML_2H]$ coordinated in the monodentate way are in fast exchange with respect to the ^{1}H NMR time scale. Equilibrium constants for the $[ML] + HL \rightleftharpoons [ML_2H]$ process were calculated on basis of the spectral changes of the ligand coordinating in the bidentate mode (Fig. 7a; Table 2).

Fig. 7

Molar fractions of [ML] and $[ML_2H]$ calculated from the chemical shifts are shown in Fig. 7b with the concentration distribution curves obtained with the help of the constants determined. The $[ML_2H]$ species can be deprotonated at higher pH values resulting in the formation of $[ML_2]$ (Chart 2) and the p*K* value of $[ML_2H]$ was also calculated based on ^{1}H NMR titrations at 1:2 metal-to-ligand ratios (Table 2). The structure of the species $[ML_2]$ of thiomaltol was geometry-optimized to energy minimum convergence by DFT calculation at B3LYP level (Chart S1). The Ru^{II}–S distances were at 2.41 and 2.46 Å for the bidentately- and monodentately-bound thiomaltolato ligands. This is slightly longer than found for Ru^{II}–S bonds as determined in single crystal X-ray diffraction analyses [21,42,43]. The C–S bond for the chelating ligand was found at 1.70 Å, while the second monodentately bound thiomaltol ligand featured a slightly longer C–S distance at 1.74 Å. In related molecular structures of Ru^{II}(arene) complexes, similar values were found for C–S bond lengths [21,42,43].

^{1}H NMR spectra were recorded at various metal-to-ligand ratios at pH 9.0 and the total concentration of the hydroxythiopyrone ligands was kept constant (Figs. S4 and S5). Under these conditions some differences between the thiomaltol and thioallomaltol systems were observed. When increasing the ligand excess to greater than two-fold a higher fraction of thioallomaltol is detected as the metal-free ligand and a lower fraction as the complex $[ML_2]$ (Fig. S4). However, a new set of signals appears in the spectra of samples containing thiomaltol suggesting the possible formation of a new kind of species and notably the same

peaks appeared in the pH-dependent spectra of samples with 1:3 metal-to-ligand ratio at pH > 8 (Fig. S6).

The p*K* values of species [ML_2H] were determined from the pH-potentiometric data besides ^{1}H NMR spectroscopy experiments (Table 2). Involvement of a tris-ligand complex [ML_3] into the speciation model significantly increased the fit between the calculated and measured titration curves in the case of thiomaltol. In the proposed structure of the thiomaltol complex [ML_3], all ligands bind in a monodentate mode (Chart 2). Similarly, tris-ligand complex of [$Ru^{II}(\eta^6\text{-}C_6Me_6)$] formed with 4-mercaptopyridine was isolated though being not able to act as chelating ligands but showing the monodentate coordination of thiolato-sulfur donor atoms in the molecular structure [42]. In order to confirm the absence of thioallomaltolato [ML_3] species, UV-Vis spectra were recorded at various metal-to-ligand ratios at pH 9.0 (Fig. S7). The addition of thioallomaltol up to a 1:2 metal-to-ligand ratio results in a blue shift of the λ_{max}, while further addition increases merely the absorbance values proportionally by the absorbance of the metal-free ligand. Therefore, the change of the absorbance at the λ_{max} shows a linear dependence from the increasing ligand concentration at M:L > 2, and the slope is similar to the molar absorptivity of the ligand, indicating that no additional species are formed in the system.

In addition, the water/Cl^- co-ligand exchange process was studied for the [$Ru^{II}(\eta^6$-*p*-cymene)(L)(H_2O)]$^+$ complex of thioallomaltol by ^{1}H NMR spectroscopy at pH 3. Similarly to the findings of the hydroxypyrone ligands (see Section 3.2), the equilibrium constant could be determined via the spectral changes and a quite similar log*K*' (H_2O/Cl^-) of 0.71(1) was obtained.

4. Conclusions

The speciation of ruthenium(II)-η^6-*p*-cymene complexes of various hydroxy(thio)pyr(id)one ligands was characterized in aqueous solution via a combined approach using pH-potentiometry, ^{1}H NMR spectroscopy and UV-Vis spectrophotometry. Significant differences in the complexation properties of the (O,O) donor hydroxypyrone and (O,S) hydroxythiopyr(id)one ligands were observed with regard to the type and stabilities of the complexes formed. Hydroxypyrones form exclusively mono-ligand complexes with moderate stability in which the ligands coordinate in a bidentate fashion. Hydrolysis of these complexes result in the formation of the neutral mixed-hydroxido species [$Ru^{II}(\eta^6$-*p*-cymene)(L)(OH)] in

the basic pH range. However, remarkable decomposition of the complex with a slow reaction rate was also found in the same pH range leading to the formation of the dinuclear trihydroxido-bridged species $[Ru_2(\eta^6\text{-}p\text{-cymene})_2(OH)_3]^+$. The hydroxythiopyr(id)one ligands form mono-ligand complexes of outstandingly high stability, which predominate in the acidic pH range. These complexes are much more cytotoxic than those of hydroxypyrones and the prominent difference in their stabilities can be related with the divergent bioactivity. The hydrolysis of hydroxythiopyr(id)one complexes (with the exception of thiodhp) at pH > 6 was found to be more complicated most probably due to the formation of poorly water soluble mixed hydroxido oligomers. These ligands are able to form bis-ligand complexes when added in excess. Under these conditions one of the ligands coordinates via the usual (O,S) mode and the other one binds in a monodentate fashion through the thione-sulfur. The $[ML_2H]$-type bis-complexes predominate at the acidic pH range and consist of the protonated ligand as the monodendate binder, while a species $[ML_2]$ is formed via the deprotonation of this ligand with increasing pH. In the case of thiomaltol, formation of the tris-complex $[ML_3]$ with ligands coordinating in a monodenate mode was also found at pH > 8. Thus, the monodenate coordination of endogenous bioligands such as the cysteine moiety of a protein should also be feasible in a biological environment.

In general the aquation of complexes of the type $[Ru^{II}(\eta^6\text{-}p\text{-cymene})(L)Cl]$ has a strong impact on the bioactivity. Therefore the Cl^-/H_2O co-ligand exchange processes were also studied and quite similar equilibrium constants were found for the Ru^{II} complexes of hydroxy(thio)pyr(id)ones. It is estimated that, e.g., in the complex of ethyl maltol ~64% of the chlorido ligand is already replaced by a water molecule at 0.1 M chloride concentration of the blood serum, and the level of aquation should increase in the intracellular fluid with its lower chloride concentration.

5. Abbreviations

allomaltol	5-hydroxy-2-methyl-4H-pyran-4-one
CT	charge transfer
deferiprone	3-hydroxy-1,2-dimethyl-pyridone
dhp	3-hydroxy-1,2-dimethyl-pyridone
ethyl maltol	2-ethyl-3-hydroxy-4-pyranone
maltol	3-hydroxy-2-methyl-4H-pyran-4-one

thioallomaltol	5-hydroxy-2-methyl-4-thiopyrone
thiodhp	3-hydroxy-1,2-dimethyl-thiopyridone
thiomaltol	3-hydroxy-2-methyl-4-thiopyrone

Acknowledgments

This work was supported by the Hungarian Research Foundation OTKA projects K77833 and 103905 and É.A. Enyedy and T. Jakusch gratefully acknowledge the financial support of J. Bolyai research fellowships. We thank Gabriella Fischer for conducting some measurements.

Appendix. Supplementary data

Supplementary data related to this article can be found online at…

References

[1] J.M. Rademaker-Lakhai, D. van den Bongard, D. Pluim, J.H. Beijnen, J.H. Schellens, Clin. Cancer Res. 10 (2004) 3717–3727.

[2] E. Alessio, G. Mestroni, A. Bergamo, G. Sava, Current Topics in Med Chem 4 (2004) 1525–1535.

[3] P. Heffeter, K. Böck, B. Atil, M.A. Reza Hoda, W. Körner, C. Bartel, U. Jungwirth, B.K. Keppler, M. Micksche, W. Berger, G. Koellensperger, J. Biol. Inorg. Chem. 5 (2010) 737−748.

[4] F.P. Dwyer, F.C. Gyarfas, W.P. Rogers, J.H. Koch, Nature 170 (1952) 190–191.

[5] W. Kandioller, A. Kurzwernhart, M. Hanif, S.M. Meier, H. Henke, B.K. Keppler, C.G. Hartinger; J. Organomet. Chem. 696 (2011) 999−1010.

[6] W. Kandioller, C.G. Hartinger, A.A. Nazarov, C. Bartel, M. Skocic, M.A. Jakupec, V.B. Arion, B.K. Keppler, Chem. Eur. J. 15 (2009) 12283–12291.

[7] J. Kljun, A.K. Bytzek,W. Kandioller, C. Bartel, M.A. Jakupec, C.G. Hartinger, B.K. Keppler, I. Turel, Organometallics 30 (2011) 2506–2512.

[8] N. Gligorijević, S. Aranđelović, L. Filipović, K. Jakovljević, R. Janković, S. Grgurić-Šipka, I. Ivanović, S. Radulović, Ž. Lj. Tešić, J. Inorg. Biochem. 108 (2012) 53–61.

[9] W.H. Ang, A. Casini, G. Sava, P.J. Dyson, J. Organomet. Chem. 696 (2011) 989–998.

[10] A.M. Pizarro, M. Melchart, A. Habtemariam, L. Salassa, F.P.A. Fabbiani, S. Parsons, P.J. Sadler, Inorg. Chem. 49 (2010) 3310–3319.

[11] F. Wang, H. Chen, S. Parsons, I.D.H. Oswald, J.E. Davidson, P.J. Sadler, Chem. Eur. J. 9 (2003) 5810–5820.

[12] F. Beckford, J. Thessing, J. Woods, J. Didion, N. Gerasimchuk, A. Gonzalez-Sarrias, N.P. Seeram, Metallomics 3 (2011) 491–502.

[13] A.F.A. Peacock, P.J. Sadler, Chem. Asian J. 3 (2008) 1890–1899.

[14] C.G. Hartinger, P.J. Dyson, Chem. Soc. Rev. 38 (2009) 391–401.

[15] H.K. Liu, P.J. Sadler, Acc. Chem. Res. 44 (2011) 349–359.

[16] P. Buglyó, E. Farkas, Dalton Trans. 39 (2009) 8063−8070.

[17] L. Bíró, E. Farkas, P. Buglyó, Dalton Trans. 39 (2010) 10272−10278.

[18] M. Hanif, H. Henke, S.M. Meier, S.Martic, M. Labib, W. Kandioller, A. Jakupec, V.B. Arion, H.B. Kraatz, B.K. Keppler, C.G. Hartinger, Inorg. Chem. 49 (2010) 7953–7963.

[19] R. Fernandez, M. Melchart, A. Habtemariam, S. Parsons, P.J. Sadler, Chem. Eur. J. 10 (2004) 5173–5179.

[20] Z. D. Liu, H. H. Khodr, D. Y. Liu, S. L. Lu, R. C. Hider, J. Med. Chem. 42 (1999) 4814–4823.

[21] W. Kandioller, C.G. Hartinger, A.A. Nazarov, M.L. Kuznetsov, R.O. John, C. Bartel, M.A. Jakupec, V.B. Arion, B.K. Keppler, Organometallics 28 (2009) 4249–4251.

[22] V. Monga, K.H. Thompson, V.G. Yuen, V. Sharma, B.O. Patrick, J.H. McNeill, C. Orvig, Inorg. Chem. 44 (2005) 2678−2688.

[23] P. Gans, A. Sabatini, A. Vacca, Talanta 43 (1996) 1739–1753.

[24] M.A. Bennett, T.N. Huang, T.W. Matheson, A.K. Smith, Inorg. Synth. 21 (1982) 74–78.

[25] L. Bíró, E. Farkas, P. Buglyó, Dalton Trans. 41 (2012) 285−291.

[26] H.M. Irving, M.G. Miles, L.D. Pettit, Anal. Chim. Acta 38 (1967) 475–488.

[27] SCQuery, The IUPAC Stability Constants Database, Academic Software (Version 5.5), Royal Society of Chemistry, 1993–2005.

[28] L. Zékány, I. Nagypál, in: Computational Methods for the Determination of Stability Constants (Ed.: D. L. Leggett), Plenum Press, New York, 1985, pp. 291–353.

[29] M.J. Frisch, G.W. Trucks, H.B. Schlegel, G.E. Scuseria, M.A. Robb, J.R. Cheeseman, G. Scalmani, V. Barone, B. Mennucci, G.A. Petersson, H. Nakatsuji, M. Caricato, X. Li, H.P. Hratchian, A.F. Izmaylov, J. Bloino, G. Zheng, J.L. Sonnenberg, M. Hada, M. Ehara, K. Toyota, R. Fukuda, J. Hasegawa, M. Ishida, T. Nakajima, Y. Honda, O. Kitao, H. Nakai, T. Vreven, J. Montgomery, J. A., J.E. Peralta, F. Ogliaro, M. Bearpark, J.J. Heyd, E. Brothers, K.N. Kudin, V.N. Staroverov, R. Kobayashi, J. Normand, K. Raghavachari, A. Rendell, J.C. Burant, S.S. Iyengar, J. Tomasi, M. Cossi, N. Rega, N.J. Millam, M. Klene, J.E. Knox, J.B. Cross, V. Bakken, C. Adamo, J. Jaramillo, R. Gomperts, R.E. Stratmann, O. Yazyev, A.J. Austin, R. Cammi, C. Pomelli, J.W. Ochterski, R.L. Martin, K. Morokuma, V.G. Zakrzewski, G.A. Voth, P. Salvador, J.J. Dannenberg, S. Dapprich, A.D. Daniels, Ö. Farkas, J.B. Foresman, J.V. Ortiz, J. Cioslowski, D.J. Fox, Gaussian 09, Revision A.02, Wallingford CT, 2009.

[30] A.D. Becke, Phys. Rev. A 38 (1988) 3098–3100.

[31] A.D. Becke, J. Chem. Phys. 98 (1993) 5648–5652.

[32] C.T. Lee, W.T. Yang, R.G. Parr, Phys Rev B 37 (1988) 785–789.

[33] G.A. Petersson, M.A. Allaham, J. Chem. Phys. 94 (1991) 6081–6090.

[34] D. Andrae, U. Haussermann, M. Dolg, H. Stoll, H. Preuss, Theor. Chim. Acta 77 (1990) 123–141.

[35] R. Dennington, T. Keith, J. Millam, GaussView, Version 5.0.8, Shawnee Mission, KS, 2009.

[36] É.A. Enyedy, O. Dömötör, E. Varga, T. Kiss, R. Trondl, C.G. Hartinger, B.K. Keppler, J. Inorg. Biochem. 117 (2012) 189−197.

[37] J. A. Lewis, B. L. Tran, D. T. Puerta, E. M. Rumberger, D. N. Hendrickson and S. M. Cohen, Dalton Trans., 2005, 2588–2596.

[38] P. Buglyó, T. Kiss, E. Kiss, D. Sanna, E. Garribba and G. Micera, Dalton Trans. (2002) 2275–2282.

[39] A.Y. Zhang, V. Monga, C. Orvig, Y.A. Wang, J. Phys. Chem. A (2008), 112(14), 3231–3238.

[40] L. Carter, D.L. Davies, J. Fawcett, D.R. Russel, Polyhedron 12 (1993) 1599−1602.

[41] E.A. Enyedy, G.M. Bognar, T. Kiss, M. Hanif, C.G. Hartinger, J. Organomet. Chem. DOI:10.1016/j.jorganchem.2012.10.042

[42] M. Gras, B. Therrien, G. Süss-Fink, P. Stepnicka, A.K. Renfrew, P.J. Dyson, J. Organomet. Chem. 693 (2008) 3419–3424.

[43] M. Hanif, P. Schaaf, W. Kandioller, M. Hejl, M.A. Jakupec, A. Roller, B.K. Keppler, C.G. Hartinger, Aust. J. Chem. 63 (2010) 1521–1528.

Legends to Figures/Charts

Chart 1 Chemical structures of the hydroxy(thio)pyr(id)one ligands

Chart 2 Proposed structures of the various complexes formed in the $[Ru^{II}(\eta^6\text{-}p\text{-cymene})Z_3]$–thiomaltol system (Z = H_2O or Cl^-)

Fig. 1 Low-field regions of the ^1H NMR spectra recorded for the $[Ru^{II}(\eta^6\text{-}p\text{-cymene})(H_2O)_3]^{2+}$–ethyl maltol system at the indicated pH values (c_L = 1 mM; M:L = 1:1; T = 25.0 °C; I = 0.20 M (KNO_3); 10% D_2O). *The inset shows the ^1H NMR chemical shifts of the CH(Ar) peaks of the p-cymene moiety in the $[Ru^{II}(\eta^6\text{-p-cymene})(L)H_2O]^+$ complex together with the fitted curves (continuous lines) in dependence of pH.*

Fig. 2 UV-Vis absorbance spectra of the $[Ru^{II}(\eta^6\text{-}p\text{-cymene})Z_3]$–ethyl maltol system recorded in the pH range of 1.9−11.5 (c_L = 0.1 mM; M:L = 1:1; T = 25.0 °C; I = 0.20 M (KCl)). *The inset shows the pH-dependence of the absorbance values at 326 nm.*

Fig. 3 High-field regions of the ^1H NMR spectra recorded for the $[Ru^{II}(\eta^6\text{-}p\text{-cymene})Z_3]$−allomaltol system at the indicated pH values (c_M = 2.1 mM; M:L = 1:1.2; T = 25.0 °C; I = 0.20 M (KCl); 10% D_2O).

Fig. 4 Bound (●) and free organometallic fragment (×) fractions for the $[Ru^{II}(\eta^6\text{-}p\text{-cymene})Z_3]$–allomaltol system calculated on basis of the ^1H NMR peak integrals of the singlet CH_3 and *i*Pr-CH_3 (*p*-cymene moiety) protons and the stability constant of the species [ML] (solid lines) (c_M = 2.1 mM; M:L = 1:1.2; T = 25.0 °C, I = 0.20 M (KCl)).

Fig. 5 UV-Vis absorbance spectra of the $[Ru^{II}(\eta^6\text{-}p\text{-cymene})Z_3]$–thioallomaltol system recorded in the pH range 0.9−11.0 (c_L = 0.06 mM; M:L = 1:1; T = 25.0 °C; I = 0.20 M (KCl/HCl) and spectra of the ligand (grey dashed line) and the metal moiety(grey line) alone for comparison at pH 2.1. *The inset shows the pH-dependence of the absorbance values at 426 nm.*

Fig. 6 Low- (a) and high-field (b) regions of the ^{1}H NMR spectra recorded for the [Ru^{II}(η^6-*p*-cymene)Z_3]−thioallomaltol system at the indicated metal-to-ligand ratios at pH 3.0 (c_L = 2.5 mM; T = 25.0 °C; I = 0.20 M (KCl); 10% D_2O). *Symbols:* i) singlet CH_3 protons of the *p*-cymene moiety ♣: non-bound metal fragment and ♣: bound metal fragment; ii) CH_3 protons of the ligand ♦: ligand bound via (O,S), ◊: ligand bound via (S) and non-bound ligand ♦: non-bound ligand alone; iii) C*H*(3) protons of the ligand ●: ligand bound via (O,S), ○: ligand bound via (S) and non-bound ligand ●: non-bound ligand alone; iv) C*H*(6) protons of the ligand ■: ligand bound via (O,S), □: ligand bound via (S) and non-bound ligand ■: non-bound ligand alone.

Fig. 7 (a) Chemical shifts of the C*H*(6) (■) and C*H*(3) (●) protons of the ligand recorded for the [Ru^{II}(η^6-*p*-cymene)Z_3]−thioallomaltol system at various metal-to-ligand ratios (pH 3.0; c_L = 2 mM; T = 25.0 °C; I = 0.20 M (KCl); 10% D_2O); (b) Concentration distribution curves for the same system calculated on basis of the chemical shifts of the C*H*(6), C*H*(3) and CH_3 protons (ML: ◊, ML_2H: ×) together with the fitted curves (dashed lines).

Table 1

Proton dissociation constants (pK_a) of the hydroxypyrone ligands; overall (logβ ($M_pL_qH_r$)), stepwise and derived stability constants of their [Ru^{II}(η^6-*p*-cymene)] complexes (T = 25 °C; I = 0.20 M (KCl)).[a]

		ethyl maltol[b]	ethyl maltol	allomaltol
pH-metry	**pK_a**	8.54(1)	8.50(1)	7.97[c]
	log β (ML)	10.07(1)	8.95(1)	8.35(1)
	log β (MLH_{-1})	–	-0.53(4)	–
	pK (ML) = log β (ML) - log β (MLH_{-1})	–	9.48	–
UV-Vis	**log β (ML)**	10.07(2)	9.01(2)	8.46(3)
	log β (MLH_{-1})	–	-0.49(2)	–
	pK (ML) log β (ML) - log β (MLH_{-1})	–	9.50	–
^{1}H NMR	**pK (ML)**	9.31(1)	9.50(4)	9.32(2)
	log$K$' (H_2O/Cl^-)[d]	–	0.74(2)	0.90(2)

[a] Uncertainties (SD) are shown in parentheses for the species described in this work. Hydrolysis products of the organometallic moiety: logβ $[Ru_2(\eta^6\text{-}p\text{-cymene})_2H_{-2}]^{2+}$ = −6.97(2) by pH-potentiometry, −7.02(5) by UV-Vis and logβ $[(Ru_2(\eta^6\text{-}p\text{-cymene})_2H_{-3}]^+$ = −11.97(1) by pH-potentiometry, −11.68(6) by UV-Vis spectroscopy.

[b] Determined at I = 0.20 M (KNO_3). Hydrolysis products: logβ $[(Ru_2(\eta^6\text{-}p\text{-cymene})_2H_{-3}]^+$ = −9.36(2) by pH-potentiometry and −9.33(2) by UV-Vis spectroscopy.

[c] Data taken from Ref. 36.

[d] $[Ru^{II}(\eta^6\text{-}p\text{-cymene})(L)(H_2O)]^+ + Cl^- \rightleftharpoons [Ru^{II}(\eta^6\text{-}p\text{-cymene})(L)(Cl)] + H_2O$ determined at various total chloride concentrations

Table 2

Proton dissociation constants (pK_a) of the hydroxythiopyr(id)one ligands; stepwise (log$K$) and derived stability constants of their [$Ru^{II}(\eta^6$-*p*-cymene)Z_3] complexes (T = 25 °C; I = 0.20 M (KCl)).[a]

		thiomaltol	thioallomaltol	thiodhp
pH-metry	**pK_a**	8.06[b]	7.64[b]	9.46(1)
	log K (ML + L = ML_2)[c]	6.93(2)[c]	7.12(4)[c]	4.36(3)[c]
	log K (ML_2 +L = ML_3)	3.2(1)	–	–
	pK_a (ML_2H)	5.68(1)	5.73(4)	8,29(3)
UV-Vis	**log K (ML)**	>14.0[d]	>13.4[d]	>13.4[d]
^{1}H NMR	**log K (ML + LH = ML_2H)**	4.54(5)	5.16(1)	3.2(2)
	pK_a (ML_2H)	6.04(1)	5.7(1)	8.47(1)
	log K (ML + L = ML_2)[c]	6.56(5)	7.1(1)	4.2(2)

[a] Uncertainties (SD) are shown in parentheses for the species characterized in this work. Hydrolysis products of the metal ion and their stability constants are given in Table 1.

[b] Data taken from Ref. 36.

[c] The equilibrium constants were calculated from the pK_a of the ligand, log K (ML + LH $\rightleftharpoons$ ML_2H) and the pK_a of ML_2H.

[d] Minimal value estimated from the UV-Vis spectrum recorded at pH 0.9 (c_L = 100 μM; M:L = 1:1)

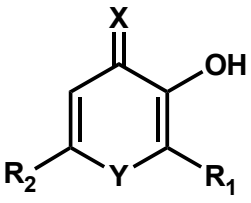

X = O; Y = O; $R_1 = CH_2\text{-}CH_3$; $R_2 = H$ ethyl maltol
X = O; Y = O; $R_1 = H$; $R_2 = CH_3$ allomaltol
X = S; Y = O; $R_1 = CH_3$; $R_2 = H$ thiomaltol
X = S; Y = O; $R_1 = H$; $R_2 = CH_3$ thioallomaltol
X = S; Y = N-CH_3; $R_1 = CH_3$; $R_2 = H$ thiodhp

Chart 1

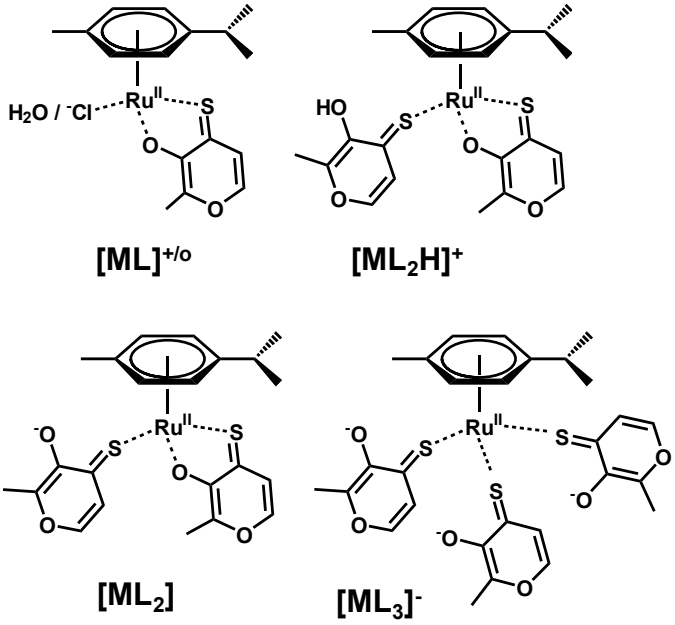

Chart 2

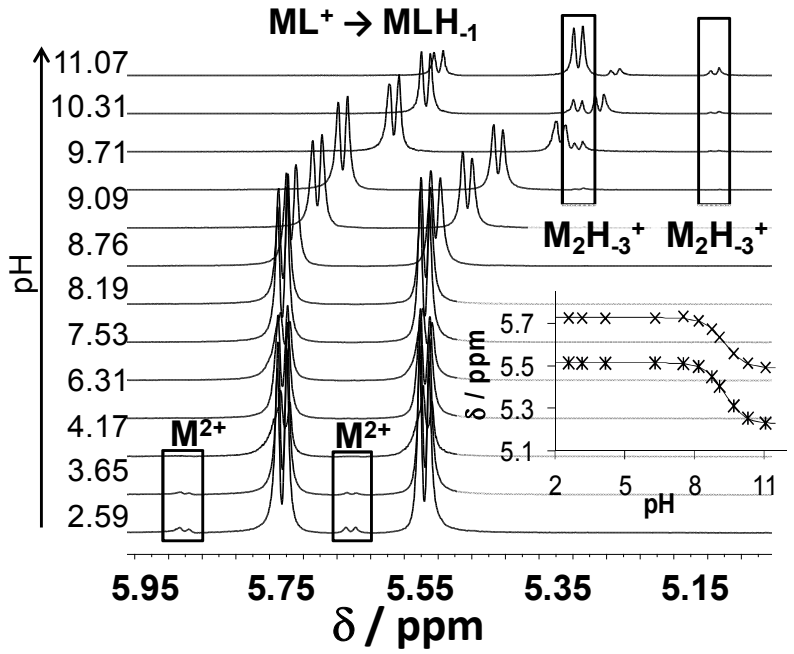
ML+ → MLH-1
11.07
10.31
9.71
9.09
8.76
8.19
7.53
6.31
4.17
3.65
2.59
pH
M2+
M2+
M2H-3+
M2H-3+
δ / ppm
5.7
5.5
5.3
5.1
2
5
8
11
pH
5.95
5.75
5.55
5.35
5.15
δ / ppm

Fig. 1

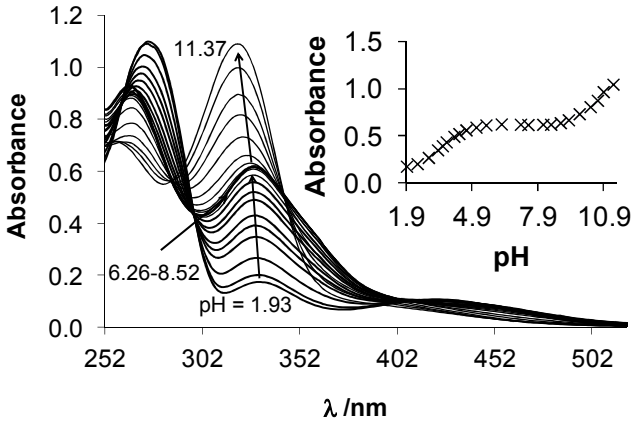
Absorbance
1.2
1.0
0.8
0.6
0.4
0.2
0.0
11.37
6.26-8.52
pH = 1.93
252
302
352
402
452
502
λ /nm
Absorbance
1.5
1.0
0.5
0.0
1.9
4.9
7.9
10.9
pH

Fig. 2

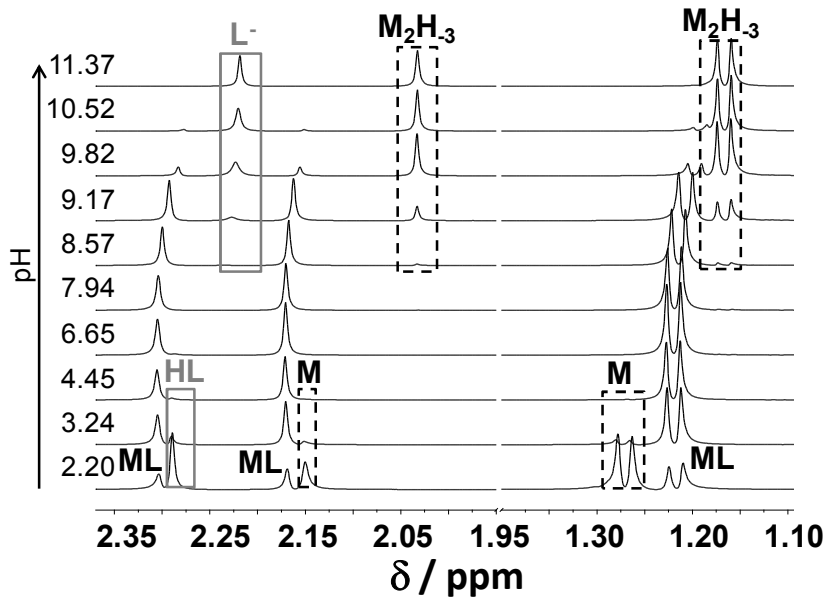
L-
M2H-3
M2H-3
11.37
10.52
9.82
9.17
8.57
7.94
6.65
4.45
3.24
2.20
pH
HL
M
M
ML
ML
ML
2.35
2.25
2.15
2.05
1.95
1.30
1.20
1.10
δ / ppm

Fig. 3

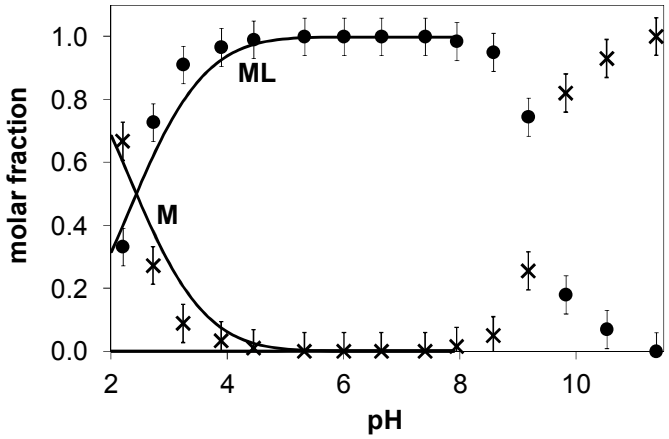
1.0
0.8
0.6
0.4
0.2
0.0
molar fraction
ML
M
2
4
6
8
10
pH

Fig. 4

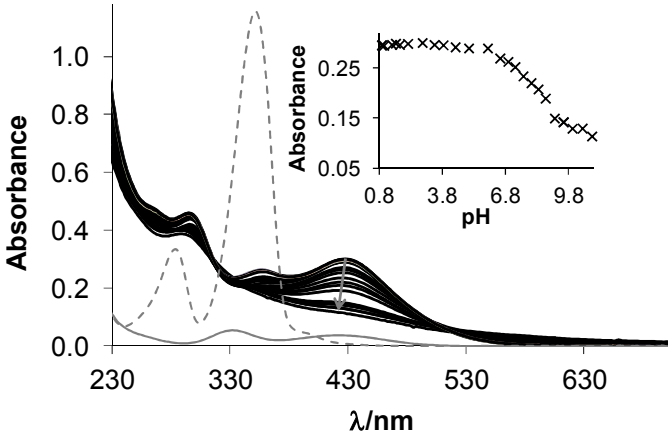
Absorbance
1.0
0.8
0.6
0.4
0.2
0.0
230
330
430
530
630
λ/nm
Absorbance
0.25
0.15
0.05
0.8
3.8
6.8
9.8
pH

Fig. 5

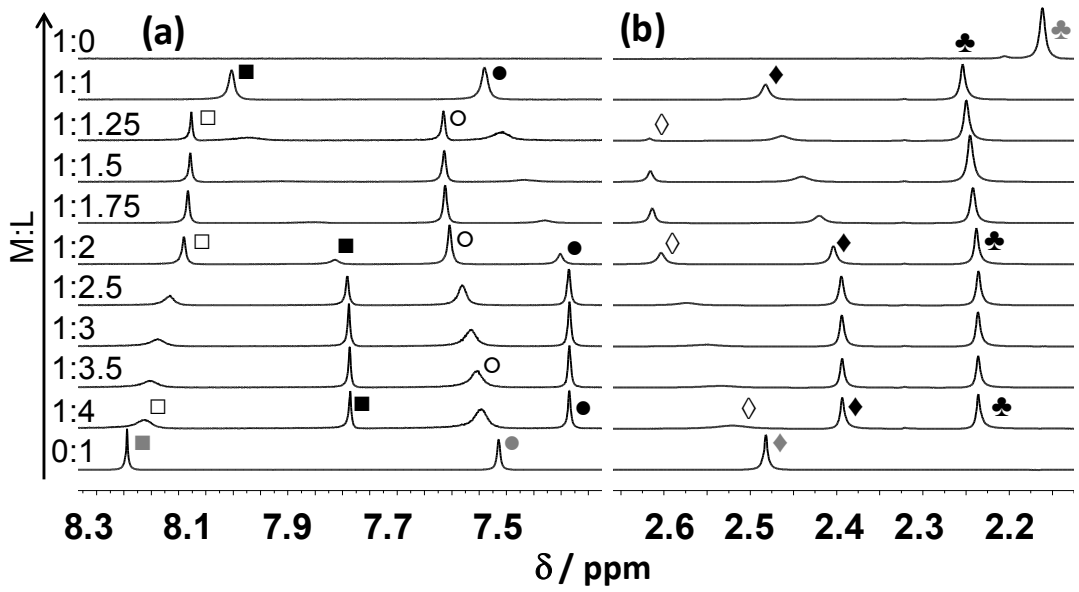
(a)
(b)
M:L
1:0
1:1
1:1.25
1:1.5
1:1.75
1:2
1:2.5
1:3
1:3.5
1:4
0:1
8.3
8.1
7.9
7.7
7.5
2.6
2.5
2.4
2.3
2.2
δ / ppm

Fig. 6

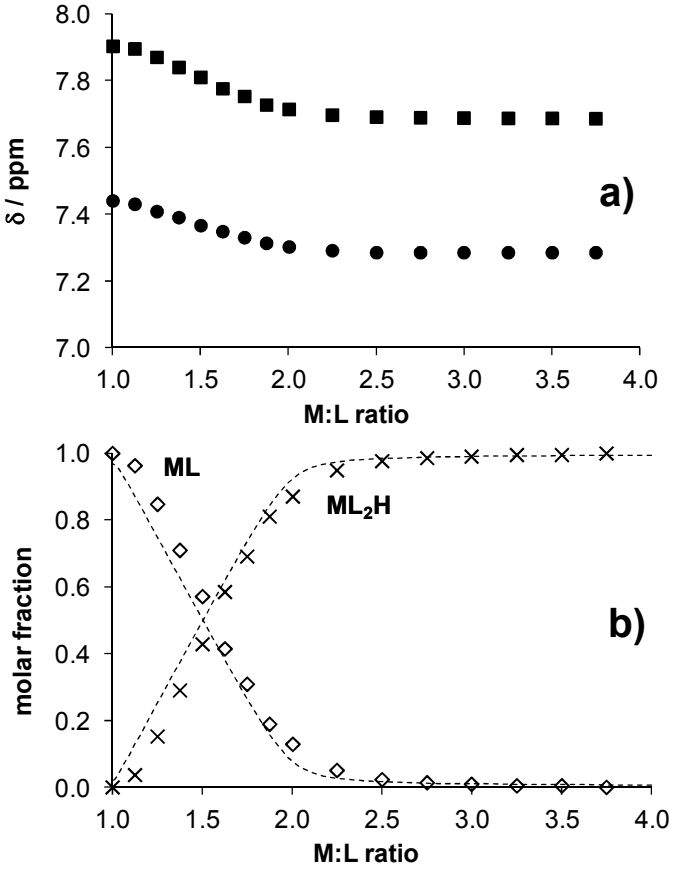
8.0
7.8
7.6
7.4
7.2
7.0
δ / ppm
a)
1.0
1.5
2.0
2.5
3.0
3.5
4.0
M:L ratio
1.0
0.8
0.6
0.4
0.2
0.0
molar fraction
ML
ML2H
b)
1.0
1.5
2.0
2.5
3.0
3.5
4.0
M:L ratio

Fig. 7